Cellular Signalling 28 (2016) 100–109

Contents lists available at ScienceDirect

Cellular Signalling

journal homepage: www.elsevier.com/locate/cellsig

Nuclear spheres modulate the expression of BEST1 and GADD45G☆

Christina Loosse [a], Magdalena Pawlas [a], Hassan S.S. Bukhari [a], Abdelouahid Maghnouj [b], Stephan Hahn [b], Katrin Marcus [c], Thorsten Müller [a,*]

[a] Cell Signaling in Neurodegeneration (CSIN), Medical Proteome-Center, Ruhr-University Bochum, 44801 Bochum, Germany
[b] Department of Molecular GI-Oncology, Clinical Research Center, Ruhr-University Bochum, Bochum, Germany
[c] Functional Proteomics, Medical Proteome-Center, Ruhr-University Bochum, 44801 Bochum, Germany

ARTICLE INFO

Article history:
Received 15 October 2015
Received in revised form 19 October 2015
Accepted 27 October 2015
Available online 28 October 2015

Keywords:
Nuclear spheres
FE65/TIP60 inducible cell line
BEST1
GADD45G
STMND1

ABSTRACT

Nuclear spheres are composed of FE65, TIP60, BLM and other yet unknown proteins. The amyloid precursor protein plays a central role for the generation of these highly toxic aggregates in the nucleus of cells. Thus, nuclear spheres might play a crucial role in Alzheimer's disease (AD). However, studies are hampered by the elevated cell death, once spheres are generated. In this work, we established for the first time a stable nuclear sphere model based on the inductive expression of FE65 and TIP60 following Doxycycline stimulation. We studied hitherto controversially discussed target genes, give clues for the reason of controversy, and moreover report new highly reliable targets bestrophin 1 and growth arrest and DNA-damage-inducible protein gamma. qPCR studies further revealed that the regulation of these targets strongly depends on the generation of nuclear spheres, but not on the induction of FE65 or TIP60 alone. As the bestrophin 1 ion channel was recently described to be involved in the abnormal release of GABA, our study might reveal the missing link between AD associated neurotransmitter changes and the amyloid precursor protein.

1. Introduction

Successive cleavage of the amyloid precursor protein (APP) through beta- (reviewed in [1]) and gamma- [2] secretases is a central hallmark of Alzheimer's disease (AD). Generated cleavage products are the soluble fragment sAPPβ, the Amyloid beta (Aβ), and the C-terminal stub CTF99. The latter fragment can be phosphorylated at several residues including T668 and Y682 (APP695 numbering), which affects the binding of APP (via the YENPTY motif) to other proteins [3]. An important adapter protein, which binds the APP C-terminal domain, is FE65 as it was suggested to submit a signal to the nucleus pointing to a receptor like function of APP. However, the role of APP T668 phosphorylation in FE65 binding and nuclear translocation has been controversially discussed. Results that single amino acid mutations at T668 reduce the interaction of APP and FE65 [4] and that the phosphorylation of T668 is essential for their interaction [4,5] are in contrast to data showing that the threonine phosphorylation liberates membrane-bound FE65 [6]. Independently of the regulatory direction of APP T668 phosphorylation for FE65 binding, which still has to be defined, the consequence is clear: the translocation of the adapter protein to the nucleus [7,8].

Another discussion in the field addresses the question if the APP intracellular domain (AICD) itself translocates into the nucleus in a Notch like manner [5] or not [9,10]. At least recent data from our lab point to the fact that AICD is not necessarily used to establish the typical FE65-dependent nuclear sphere phenotype [11], which is the final consequence of a disturbed interaction of the adapter protein to APP or its C-terminal cleavage products. Once generated as small spherical structures in the nucleus, these complexes grow and fuse together and are finally detectable as structures of about 2 μm in size, which was detectable in a similar manner by a Swiss group following pharmacological inhibition of transcription [12]. Other known components of nuclear spheres are the histone acetyltransferase TIP60 [13,14] and the bloom syndrome protein BLM, a DNA helicase [11]. Notably, endogenous AICD positive nuclear aggregates, which potentially correspond to nuclear spheres, could be identified in primary neurons following nuclear export blockade [15], but the function of the structures is largely unknown and evidence for the existence of nuclear spheres in human samples is missing until now. However, cell culture data points to the possible impact of the aggregates for several central mechanisms. A couple of publications points to a role for FE65-dependent complexes in gene transcription, e.g. as a feedback mechanism in the regulation of APP [16], expression changes for cytoskeletal associated genes [17,14], the tetraspanin KAI1 [18] or the glycogen synthase kinase-3beta [19], which is one of the kinases phosphorylating the TAU protein [20]. The illustrated gene expression changes, especially the role of a sequestered AICD fragment, which was suggested to be rapidly degraded, has been highly controversially discussed [21,10] and it was suggested that instead of AICD cleavage the phosphorylation of the APP C-terminus is essential for FE65-dependent signaling function [11].

☆ The authors declare that they have no conflict of interest..

* Corresponding author at: Medizinisches Proteom-Center, Ruhr-University Bochum, D-44801 Bochum, Germany.
E-mail address: thorsten.t.mueller@rub.de (T. Müller).

http://dx.doi.org/10.1016/j.cellsig.2015.10.019
0898-6568/

Second, nuclear spheres might play a pivotal role in DNA repair. FE65, a central component of the spherical structures, has been shown to be involved in TIP60-dependent histone acetylation at DNA double strand breaks [22,23] and a C-terminal APP fragment was shown to induce apoptosis via TIP60 [24]. Notably, the DNA damage associated mechanism was suggested to be in close communication to the aforementioned gene expression changes as it could be shown that FE65 was enriched in promoter regions of genes linked to DNA damage in a genome-wide location analysis [25].

Finally, a function of FE65 in cell cycle progression was discussed as a consequence of its impact on the expression of thymidylate synthase [26] and other cell cycle genes [25]. In combination with BLM, which we identified as another component of nuclear spheres, we also discussed a role of nuclear spheres in proliferation and potential cell cycle re-entry [11].

Taken together nuclear spheres could play a crucial role in important cellular mechanisms that might contribute to neurodegeneration. Controversial findings are in part the consequence of a variety of different approaches that have been used in the past, e.g. combination of AICD with FE65, AICD with TIP60, AICD with FE65 and TIP60, or a single protein alone. Assuming that the generation of nuclear spheres composed of FE65 and TIP60 is the consequence of APP signaling to the nucleus we now developed and studied an inducible model for the co-expression of both proteins, which shows the expected phenotype of nuclear spheres.

2. Materials and methods

2.1. Primers

Primers that were used for PCR and qPCR are listed in the Supplementary Table S-1.

2.2. Plasmid construction

Plasmid pBI_FE65-EGFP_TIP60_G418 was obtained by excising the Ampicillin cassette from the pBI_FE65-EGFP_TIP60 plasmid using the restriction enzymes BstEII and BsaI and replacing it by the Kanamycin/G418 cassette that was obtained via PCR from the pEGFP-N1 (Clontech, France) vector with the primers G418 forward (fwd) and G418 reverse (rev). The pTet-On_Blas plasmid was prepared with the help of the In-Fusion®HD cloning kit (Clontech) according to the manufacturer's instructions. The pTet-On vector (Clontech) was linearized via PCR with the primers pTet-On fwd and pTet-On rev whereby the Ampicillin cassette was excluded. The Blasticidin cassette was amplified from the vector pCDNA-6TR (Life Technologies, Germany) with the primers Blas fwd and Blas rev that showed complement overhangs for the linearized pTet-On plasmid.

2.3. Cell culture

The inducible FE65-EGFP/TIP60 expressing cell line was established by transfecting the before mentioned plasmids into HEK293 cells. Therefore, 1×10^6 cells were seeded on a 10 cm cell culture dish and cultured in Dulbecco's modified eagle medium (DMEM, Gibco®/Life Technologies, Germany) supplemented with 10% fetal bovine serum (FBS, Gibco®/Life Technologies) and 1% Penicillin/Streptomycin (PenStrep, Gibco®/Life Technologies) in 37 °C and 5% CO_2. After 24 h transfection was performed using Polyethylenimine (PEI). 5 ml serum free DMEM plus 1% PS were mixed with 20 μg DNA and 120 μg PEI and incubated for 17 min at room temperature. Medium was aspirated and cells were washed once with Dulbecco's phosphate buffered saline +/+ (DPBS, Gibco®/Life Technologies) before the DNA–PEI-mixture was added to the cells and incubated for 4 h in 37 °C and 5% CO_2. Then, the mixture was replaced by normal medium and cells were incubated in 37 °C and 5% CO_2. In order to get rid of untransfected cells, 1000 μg/ml Geneticin (G418) and 10 μg/ml Blasticidin were added to the medium 24 h after transfection. Selection medium was replaced every day. After 7–12 days single colonies were isolated and grown in a 24 well plate. Therefore, DMEM of untransfected cells was filtered through a Filtropur S 0.2 sterile filter (Sarstedt, Germany), supplemented with 1000 μg/ml G418 and 10 μg/ml Blasticidin, and added to the cells. The mother plate was induced with 2 μg/ml Doxycycline and respective glowing clones were transferred from 24 wells to larger cell culture dishes.

For microscopy, cells were induced with 2 μg/ml Doxycycline for 48 h and were analyzed by fluorescence microscopy (IX50, Olympus, Germany). Pictures were taken with a SLR camera (Olympus) and CellP software (Olympus).

2.4. Cell lysis

For each clone, two 10 cm cell culture dishes were seeded with 2×10^6 cells each and always one plate was induced with 2 μg/ml Doxycycline. Cells were cultivated in 10 ml DMEM supplemented with 10% FBS, 1% PenStrep, 1000 μg/ml Geneticin and 10 μg/ml Blasticidin at 37 °C and 5% CO_2 for 48 h. After incubation medium was aspirated and cells were washed with DPBS (+/+) and subsequently harvested with trypsin (Gibco®/Life Technologies). After centrifugation (300 ×*g*, 5 min, room temperature) the cell pellet was resuspended in 1 ml DPBS (+/+). 100 μl was used for RNA isolation and 900 μl for protein isolation. DPBS (+/+) was removed by centrifugation (500 ×*g*, 5 min, room temperature). For protein isolation, cell pellets were resuspended in 200 μl 1% Triton X-100 in DPBS (+/+) and sonicated, and cellular extracts were centrifuged for 15 min at 16,000 ×*g* at 4 °C. The supernatants were collected and protein concentration was measured by the Bradford assay.

2.5. Immunoblotting

25 μg of total protein extracts was separated via SDS-PAGE using a 12% BisTris gel. Then proteins were transferred to a nitrocellulose membrane. After blocking the membrane with Starting Block™ TBS (Thermo Scientific, Germany) the blot was probed with the following antibodies diluted in Starting Block™ TBS: 1:1000 anti-FE65 antibody (Millipore, Germany), 1:500 anti-TIP60 antibody (Cell Signaling, The Netherlands), 1:500 anti-GFP antibody (Santa Cruz, USA) and 1:5000 anti-GAPDH (Genetex, USA) as a reference. IR Dye™ 680 and IR Dye™ 800 CW (Li-Cor, USA) 1:15,000 were used as secondary antibodies. For protein detection and quantification the Odyssey Infrared Imaging system was used with the Odyssey Application Software version 3.0.21 (LiCor).

2.6. In gel protein digestion

For spectral counting analysis 25 μg of total protein extracts was shortly migrated into a 12% BisTris gel. The protein including gel pieces were excised, cut into small pieces, alternately washed with buffer A (50 mM ammonium hydrogen carbonate (NH_4HCO_3)) and buffer B (50 mM NH_4HCO_3/50% ACN (acetonitrile)), reduced using DTT (dithiothreitol), alkylated using iodoacetamide and again alternately washed with buffer A and buffer B. Following dehydration of gel pieces, trypsin (Serva, Germany) was solved in 10 mM HCl and 50 mM NH_4HCO_3 and was used for overnight in gel digestion at 37 °C (trypsin:protein ratio 1:20). Peptides were then extracted once with 200 μl of 50% ACN/0.05% TFA (trifluoroacetic acid) and once with 100 μl of 50% ACN/0.05% TFA. Extracts were combined and centrifuged for 5 min at 16,000 ×*g*. The supernatant was transferred to a new vial in order to get rid of potential gel residuals. Then, ACN was removed in vacuo. For LC–MS analysis, a final volume of 100 μl was prepared by the addition of 0.1% TFA and peptide concentration was measured with amino acid analysis.

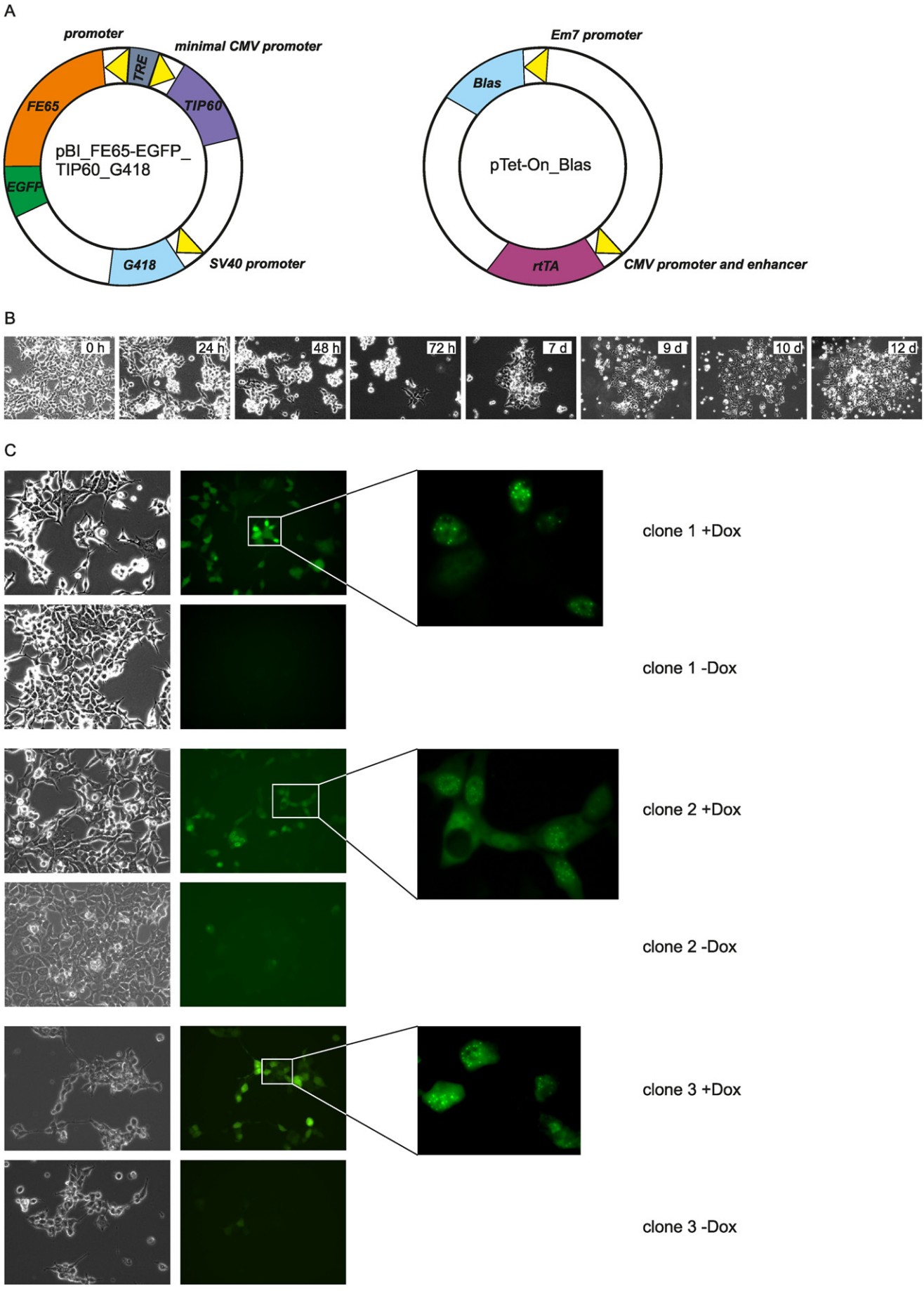
A
promoter
minimal CMV promoter
TRE
FE65
TIP60
pBI_FE65-EGFP_
TIP60_G418
EGFP
G418
SV40 promoter
Em7 promoter
Blas
pTet-On_Blas
rtTA
CMV promoter and enhancer
B
0 h
24 h
48 h
72 h
7 d
9 d
10 d
12 d
C
clone 1 +Dox
clone 1 -Dox
clone 2 +Dox
clone 2 -Dox
clone 3 +Dox
clone 3 -Dox

For identification of the corresponding Western blot signals 25 μg of total protein extracts was separated in a 12% BisTris gel. After Coomassie staining and destaining respective gels bands were excised, cut into small pieces, alternately washed with buffer A and B, dehydrated in vacuo and digested with trypsin over night at 37 °C (trypsin:protein ratio 1:25). Peptide extraction was performed as described above. For LC–MS analysis, a final volume of 50 μl was prepared by the addition of 0.1% TFA and peptide concentration was measured with amino acid analysis.

2.7. Mass spectrometry

200 ng of peptide extracts was used for mass spectrometry analysis. Samples for subsequent spectral counting analysis were injected via the autosampler of an RSLC nano system (Thermo Scientific), concentrated on a C_{18} trapping column (2 cm length, 100 μm i.d., 5 μm particle size, Thermo Scientific), and separated on a C_{18} analytical column (50 cm length, 75 μm i.d., 2 μm particle size, Thermo Scientific) heated at 60 °C before being emitted via a coated silica tip (FS360-20-10-D-20, New Objective, USA) of the Nanospray Ionization (NSI) source of an Orbitrap Elite (Thermo Scientific). The HPLC separation was performed with a gradient method of in total 120 min consisting of: 7 min of loading the sample and washing the column with 0.1% TFA at a flow rate of 30 μl min^{-1} on the trapping column, followed by separation applying a linear gradient at a flow rate of 400 nl min^{-1} with the solvents A (0.1% FA (formic acid) in HPLC grade water) and B (84% ACN/0.1% FA in HPLC grade water) starting from 5% B to 40% B in 98 min on the heated analytical column, a linear gradient of 40% B to 95% B in 2 min, and washing for 7 min with 95% B. Finally, a gradient was applied from 95% B to 5% B in 1 min followed by equilibration for 5 min with 5% B. For ionization a spray voltage of 1.5 kV and capillary temperature of 275 °C was used. The acquisition method consisted of two scan events, Full MS and MS/MS. The Full MS was monitored from m/z 300 to 2000, with an Orbitrap resolution of 60,000 (at m/z 400), a maximum injection time of 200 ms and an automatic gain control (AGC) value of 1e6. The m/z values initiating MS/MS were set on a dynamic exclusion list for 35 s. Lock mass polydimethylcyclosiloxane (m/z 445.120) was used for internal recalibration. The 20 most intensive ions (charge >1) were selected for MS/MS-fragmentation and scanned in the normal scan mode in the ion trap, with a maximum injection time of 100 ms and an AGC value of 1e4. Fragments were generated by low-energy collision-induced dissociation (CID) on isolated ions with collision energy of 35%.

Samples for sole identification were injected via the autosampler of an RSLC nano system (Thermo Scientific), concentrated on a C_{18} trapping column (2 cm length, 100 μm i.d., 5 μm particle size, Thermo Scientific), and separated on a C_{18} analytical column (25 cm length, 75 μm i.d., 2 μm particle size, Thermo Scientific) heated at 60 °C before being emitted via a coated silica tip (FS360-20-10-D-20, New Objective) of the NSI source of an LTQ Velos Pro (Thermo Scientific). The HPLC separation and ionization were performed as described above. The acquisition method consisted of two scan events, Full MS and MS/MS. The Full MS was monitored in the enhanced scan mode from m/z 300 to 1500, a maximum injection time of 10 ms and an AGC value of 3e4. The m/z values initiating MS/MS were set on a dynamic exclusion list for 35 s. The 10 most intensive ions (charge >1) were selected for MS/MS-fragmentation and scanned in the rapid scan mode in the ion trap, with a maximum injection time of 100 ms and an AGC value of 1e4. Fragments were generated by low-energy CID on isolated ions with collision energy of 35%.

2.8. Database searches

For subsequent spectral counting analysis, .raw files were processed in Proteome Discoverer 1.4 and analyzed using the Mascot search algorithm with a mass tolerance of 5 ppm and a fragment mass tolerance of 0.4 Da. Searches were performed allowing two missed cleavage sites after tryptic digestion. Carbamidomethylation (C) was considered as fixed modification, oxidation (M) as variable modification. All data were searched against a database created by DecoyDatabaseBuilder [27] containing the whole Uniprot/Swissprot of the taxonomy *Homo sapiens* (release 2014_10, 20,194 entries) with one additional shuffled decoy for each protein.

For peptide identification in specific gel bands .raw files were processed in Proteome Discoverer 1.4 and analyzed using the Mascot search algorithm with a mass tolerance of 0.4 Da and a fragment mass tolerance of 0.4 Da. Searches were performed allowing one missed cleavage site after tryptic digestion. Oxidation (M) and propionamide (C) were considered as variable modifications. Targeted Decoy PSM Validator was implemented with an FDR of 1%. All data were searched against a database containing the whole Uniprot/Swissprot entries (release 2015_05, 548,454 entries).

2.9. Spectral counting

For spectral counting identified peptides were further processed using the PIA algorithm [28]. An FDR-threshold of 1% was applied and a list of all peptide spectrum matches (PSMs) was extracted. These PSMs were further processed using the Pivot table function of Microsoft Excel resulting in a table representing spectral counts for every peptide belonging to a certain protein. Processed spectral counts (PSCs) based on spectral and peptide counts were calculated as described previously [29,11] and subsequently used as basis for label-free quantification. In brief, PSC calculation was performed by summing up all spectral counts for unique peptides belonging to the respective protein. To determine the fold change of the expression of FE65 and TIP60 the ratio between the averaged spectral indices of the induced samples and non-induced samples was calculated and Student's *t*-test was conducted for significance estimation.

2.10. RNA extraction, cDNA synthesis, quantitative PCR (qPCR)

RNA lysates from cell culture were extracted with the help of the GF-1 Total RNA Extraction Kit (Vivantis, USA) according to the manufacturer's instructions. Therefore, 2×10^6 cells of each clone (induced vs. non-induced) were seeded on a 10 cm cell culture dish and grown for 48 h and 1/10 of the cells were used for RNA extraction.

cDNA synthesis was performed using the RevertAid First Strand cDNA Synthesis Kit (Thermo Scientific) and random hexamer primers according to the manufacturer's instructions. 11 μl RNA were used and synthesis conditions were as follows: 5 min at 25 °C, 60 min at 42 °C and 5 min at 70 °C.

mRNA levels of *FE65* and *TIP60* were determined using a SYBR Green real-time PCR assay on a RotorGene Q device (Qiagen, Germany). 0.1 μl

Fig. 1. Generation of FE65-EGFP/TIP60 inducible stable cell lines. (A) *FE65* and *TIP60* were cloned into a pBI vector that carries a Tetracycline response element (TRE) and a bidirectional promoter, which allows induction of gene expression dependent on the presence of Doxycycline. Thereby, *FE65* was fused to *EGFP* (enhanced green fluorescent protein) and furthermore, the Ampicillin resistance was replaced by a Geneticin/Kanamycin resistance cassette (G418) resulting in the plasmid pBI_FE65-EGFP_TIP60_G418. The pTet-On plasmid, which carries the reverse Tetracycline-controlled transactivator (rtTA) was modified by replacing the Ampicillin resistance by a Blasticidin resistance cassette (Blas) resulting in the plasmid pTet-On_Blas. The Kanamycin cassette, which is also part of the vector, was not changed. (B) The plasmids pBI_FE65-EGFP_TIP60_G418 and pTet-On_Blas were co-transfected into HEK293 cells. After 24 h of transfection cells were treated with 1000 μg/ml G418 and 10 μg/ml Blasticidin. After 24 h of treatment untransfected cells started to die and after 72 h small colonies remained that grew bigger after 7–12 days. (C) Example of three isolated colonies (clone 1–3) that were cultivated. Cells were induced for 48 h with Doxycycline (+Dox) and more than 70–95% of the cells were EGFP positive depending on the different clones. The zoom in shows that several cells revealed the typical FE65/TIP60 sphere phenotype. For the zoomed image of clone 1 the exposure time was reduced in order to make spheres visible. Non-induced cells (−Dox) are shown as control and were almost completely EGFP negative.

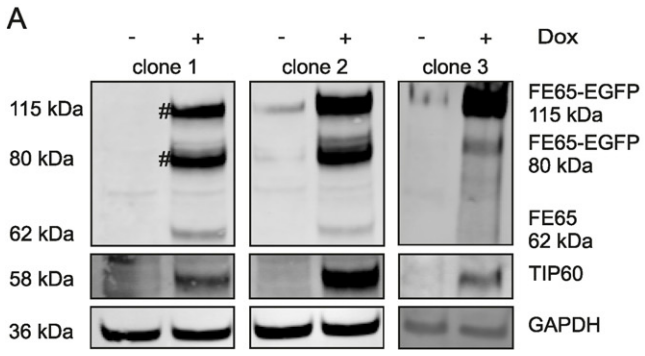
A
- + - + - + Dox
clone 1
clone 2
clone 3
115 kDa
80 kDa
62 kDa
58 kDa
36 kDa
#
#
FE65-EGFP 115 kDa
FE65-EGFP 80 kDa
FE65 62 kDa
TIP60
GAPDH

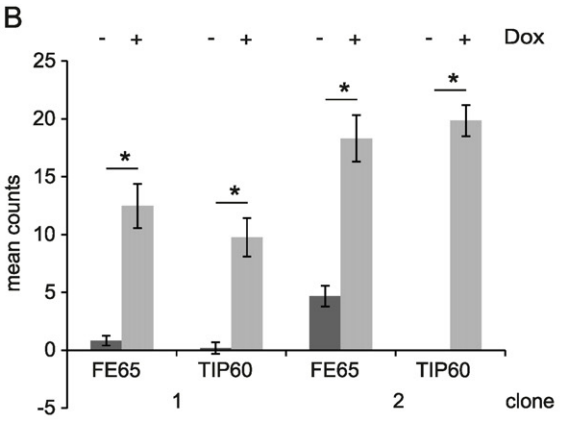
B
- + - + - + - + Dox
mean counts
25
20
15
10
5
0
-5
*
*
*
*
FE65
TIP60
FE65
TIP60
1
2
clone

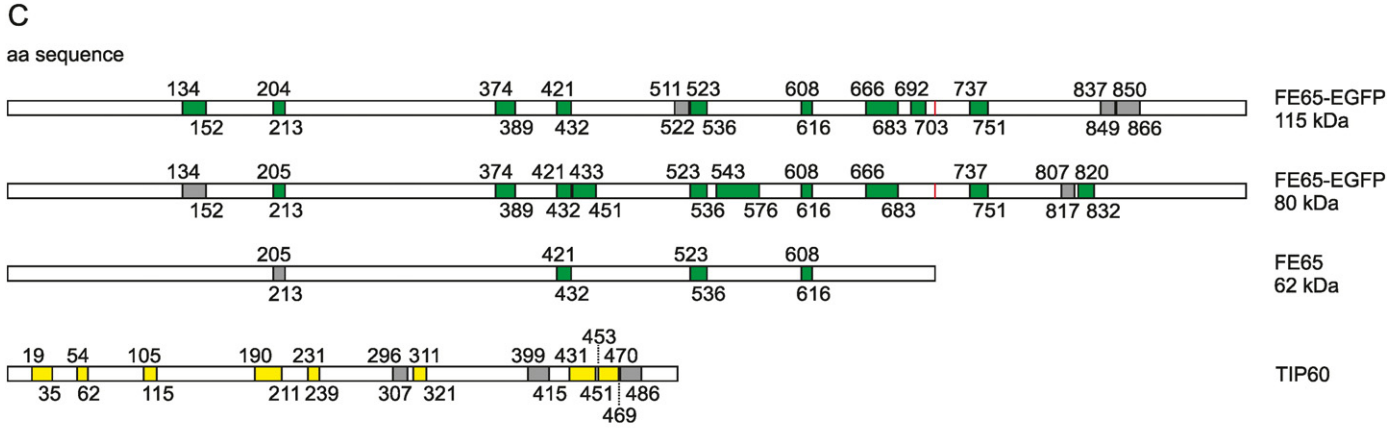
C
aa sequence
134 204 374 421 511 523 608 666 692 737 837 850
152 213 389 432 522 536 616 683 703 751 849 866
FE65-EGFP 115 kDa
134 205 374 421 433 523 543 608 666 737 807 820
152 213 389 432 451 536 576 616 683 751 817 832
FE65-EGFP 80 kDa
205 421 523 608
213 432 536 616
FE65 62 kDa
19 54 105 190 231 296 311 399 431 453 470
35 62 115 211 239 307 321 415 451 469 486
TIP60

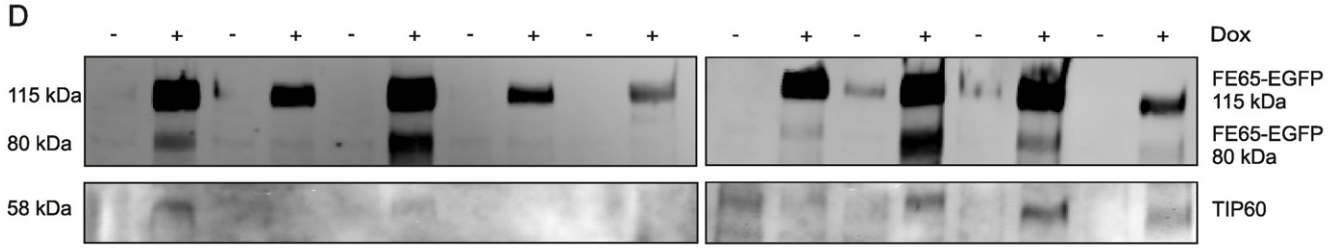
D
- + - + - + - + - + - + - + - + - + - + Dox
115 kDa
80 kDa
58 kDa
FE65-EGFP 115 kDa
FE65-EGFP 80 kDa
TIP60

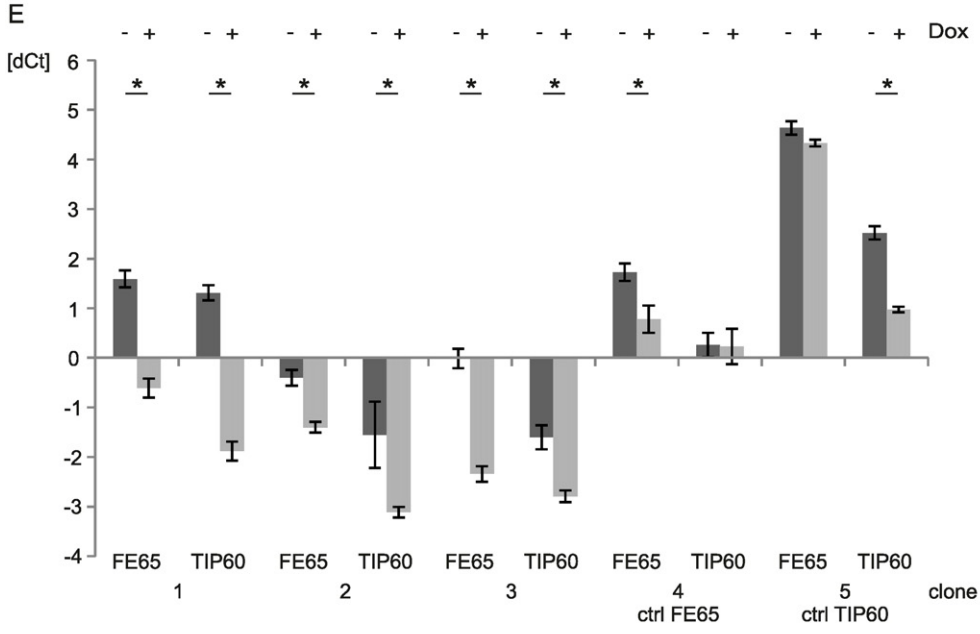
E
- + - + - + - + - + - + - + - + - + - + Dox
[dCt]
6
5
4
3
2
1
0
-1
-2
-3
-4
*
FE65 TIP60 FE65 TIP60 FE65 TIP60 FE65 TIP60 FE65 TIP60
1 2 3 4 5 clone
ctrl FE65
ctrl TIP60

of template cDNA was mixed with 4.5 μM of each corresponding primer, 10 μl SYBR® Premix Ex Taq™ II (Tli RNase H Plus) (Clontech) and 7.9 μl H_2O. Cycling conditions were as follows: initial 95 °C for 30 s followed by 45 cycles of 95 °C for 30 s, 56 °C for 30 s, and 72 °C for 30 s. Those cycles were followed by acquisition of a melting curve. Each clone was measured in triplicate and *GAPDH* was used as reference for dCt calculation. Data evaluation was done with the RotorGene Q Series Software (Qiagen). Gene expression was calculated according the method of Livak and Schmittgen [30]. The same qPCR procedure was used for quantification of target gene mRNA levels of GSK3β, KAI1, APP, PTCH1, WASF1, RIMKLB, NEURL3, KIAA0408, BEST1, STMND1, NPPB, SNHG12, BEX1, MATN1-AS1, TMEM198, PVT1, MMP24, KRT80, STMN4, LOC643201, CYTIP, XPA, EMC9, MIR7-3HG, LRP5L, PHF21B, WISP2, KCNN4, PTPRH, SNAP25, ETV5, PER2, CREB5, NFKB2, FOS, SF1, GADD45G, and ZYMND8.

2.11. mRNA expression analyses and data processing

100 ng of each total RNA sample was hybridized to Agilent whole genome expression microarrays (Human GE 4x44K, v2 G4845A, AMADID 026652, Agilent Technologies, USA). mRNA labeling, hybridization and washing were carried out according to the manufacturer's instructions. Images of hybridized microarrays were acquired with a DNA microarray scanner (Agilent G2505B) and features were extracted using the Agilent Feature Extraction image analysis software (AFE) version A.10.7.3.1 with default protocols and settings. The AFE algorithm generates a single intensity measure for each microRNA, referred to as the total gene signal (TGS), which was used for further data analyses using the GeneSpring GX software package version 13.1. AFE-TGS were normalized by the quantile method. Subsequently, data were filtered on normalized expression values. Only entities, which had values within the selected cutoff (50th–100th percentile), were further included in the data analysis process. A pairwise comparison of measured mRNA levels of induced clone 1 versus non-induced clone 1, respectively, was performed. We conducted moderated *t*-test, unpaired, assuming equal variances using GeneSpring GX software package version 13.1. The p-values were adjusted for multiple testing according to Benjamini and Hochberg [FDR] and results were considered statistically significant at adjusted p-values below 0.05. Furthermore, only mRNAs with fold change ≥2.5 in the microarray analyses were considered worthy of more in-depth analyses.

3. Results

3.1. Stable clones inducible for FE65/TIP60 reveal the nuclear sphere like phenotype and FE65 fragmentation

Nuclear spheres are currently discussed to contribute to neurodegeneration by a yet unknown mechanism. In order to study these spherical structures in detail, it was our aim to establish an appropriate stable cell culture model. As outlined in our previous work [11], expression of FE65 is sufficient to establish the nuclear sphere phenotype but co-expression of TIP60 significantly enhances the generation of the nuclear complexes. Thus we intended to generate a stable FE65/TIP60 co-expression model. As CMV promoter driven experiments caused enormous death in affected HEK293 cells within a short time (not shown) we went for an inducible cell culture model comprising the advantages of moderate FE65/TIP60 expression levels (instead of high-level artificial over-expression) as well as precise control of expression by the applied component Doxycycline (Dox).

For the generation of stable cell lines we initially cloned human FE65 tagged with EGFP and TIP60 in the pBI vector (Clontech, France) under the control of the bidirectional TRE promoter (Fig. 1A). Furthermore the Ampicillin cassette was exchanged for the G418/Kanamycin selection cassette for subsequent selection of positively transfected cells. The pTet-On vector (Clontech) carrying the reverse Tetracycline-controlled transactivator (rtTA) was modified by replacing the Ampicillin resistance by a Blasticidin resistance cassette (Blas). Both vectors were simultaneously transfected in HEK293 cells, which can be easily selected for G418 and Blasticidin (Fig. 1B). Positive clones were initially identified by a positive EGFP signal and the presence of the nuclear sphere phenotype in induced (+Dox) vs. non-induced cells (−Dox, Fig. 1C). In total, we were able to establish 12 stable clones, which were subsequently further characterized. Immunoblotting revealed significantly elevated protein abundances for three exemplary studied clones for FE65 and TIP60 following induction (+Dox) as expected (Fig. 2A). Notably, putative FE65-EGFP cleavage products were detectable with a molecular weight of about 80 and 62 kDa in size, which might be a consequence of the described caspase-dependent (Saeki 2011) or endoproteolytic (Hu 2005) FE65 cleavage. FE65 cleavage is elevated in the presence of TIP60 with significantly more 80 kDa cleavage product in samples that co-express TIP60 compared to samples without TIP60 expression ($p < 0.005$, Fig. 2D) pointing to the fact that TIP60 induced FE65 fragmentation. Consistently, using anti GFP antibody the two largest FE65 signals (# labeled in Fig. 2A) could be detected but not FE65 62 kDa (SupplementaryFig. S-1). In good agreement to the immunoblot data, mass spectrometry/spectral count based data analysis revealed moderate to high induction of both proteins in clones 1 and 2 (Fig. 2B, regulation factors are given in the figure supplement).

In order to identify potential FE65 cleavage products, mass spectrometry for gel pieces corresponding to positive immunoblot signals for FE65 (and TIP60) was applied. Mass spectrometry analysis proved previous immunoblot data, identifying FE65 and EGFP tryptic peptides for the 115 and 80 kDa signals but only FE65 peptides in the gel piece corresponding to the 62 kDa signal (Fig. 2C). For TIP60, which was identified by MS with high sequence coverage, we detected no cleavage products underlining specificity of FE65 cleavage instead of unspecific protein degradation. FE65 and TIP60 expression was further analyzed in the established stable clones using quantitative PCR (qPCR, Fig. 2E, dCt values are illustrated). Induction ratios of 1.9–5.0 for FE65 and 2.3–9.1 for TIP60 revealed moderate over-expression, which fits to our expectation as high levels of both proteins would cause cell death.

Fig. 2. Characterization of FE65-EGFP/TIP60 inducible stable cell lines. (A) Immunoblotting of three exemplary shown clones revealed prominent FE65 and TIP60 protein levels upon 48 h of induction. Nitrocellulose membrane was probed with anti-FE65 antibody (1:1000, Millipore), anti-TIP60 antibody (1:500, Cell Signaling) and anti-GAPDH antibody (1:5000, Genetex) as reference. FE65 revealed three signals for 48 h induced clones 1 and 2 and two signals for clone 3 (+Dox), whereas no or faint signal was detectable in the control conditions (−Dox). TIP60 revealed a prominent signal in all three induced clones but no signal in control cells. In the #-marked FE65 signals EGFP was also detected via immunoblotting (compare SupplementaryFig. S-1). (B) Mass spectrometry combined with spectral counting based data analysis proved the upregulation of FE65 and TIP60. For the induced cells (+Dox) significantly more spectra (mean counts) were acquired for FE65 and TIP60 compared to control cells (−Dox) ($p < 0.05 \times 10^{-5}$, $n = 6$ technical replicates). Spectral counting based data analysis revealed regulation factors of 12.51 (±1.94, s.d.) for FE65 and 9.47 (±1.64, s.d.) for TIP60 in clone 1 and 4.02 (±0.8, s.d.) for FE65 and 19.84 (±1.25, s.d.) for TIP60 in clone 2 (missing values were set to 1). (C) Gel pieces corresponding to FE65 (115 kDa, 80 kDa, 62 kDa) and TIP60 signals (compare to A) were excised, tryptically digested and identified via mass spectrometry. Schematic amino acid (aa) sequences of the theoretical proteins are given. The red line marks the fusion site of FE65 and EGFP. Identified peptides for FE65 (−EGFP) are displayed in green and for TIP60 in yellow. Gray colored peptides indicate peptides that were identified with poor quality spectra. Numbers above the aa sequence denote the starting position of a peptide, numbers below the end position of a peptide. (D) FE65 cleavage was significantly elevated when also TIP60 was expressed ($p < 0.005$). (E) *FE65* and *TIP60* expression (studied in three different clones) was significantly upregulated in induced cells (+Dox) compared to control cells (−Dox) ($p < 0.05 \times 10^{-4}$, $n = 3$ technical replicates for each clone, calculation of regulation factors according to ddCt method [30]: clone 1 FE65 4.59 (±0.78, s.d.), TIP60 9.13 (±1.50, s.d.)/clone 2 FE65 2.01 (±0.25, s.d.), TIP60 3.22 (±1.20, s.d.)/clone 3 FE65 5.03 (±0.83, s.d.), TIP60 2.28 (±0.40, s.d.)). dCt values were calculated using *GAPDH* as reference. Clone 4 corresponds to a control clone that induces just *FE65* (1.93 (±0.43, s.d.)), whereas clone 5 is inducible for just *TIP60* (2.91 (±0.27, s.d.)).

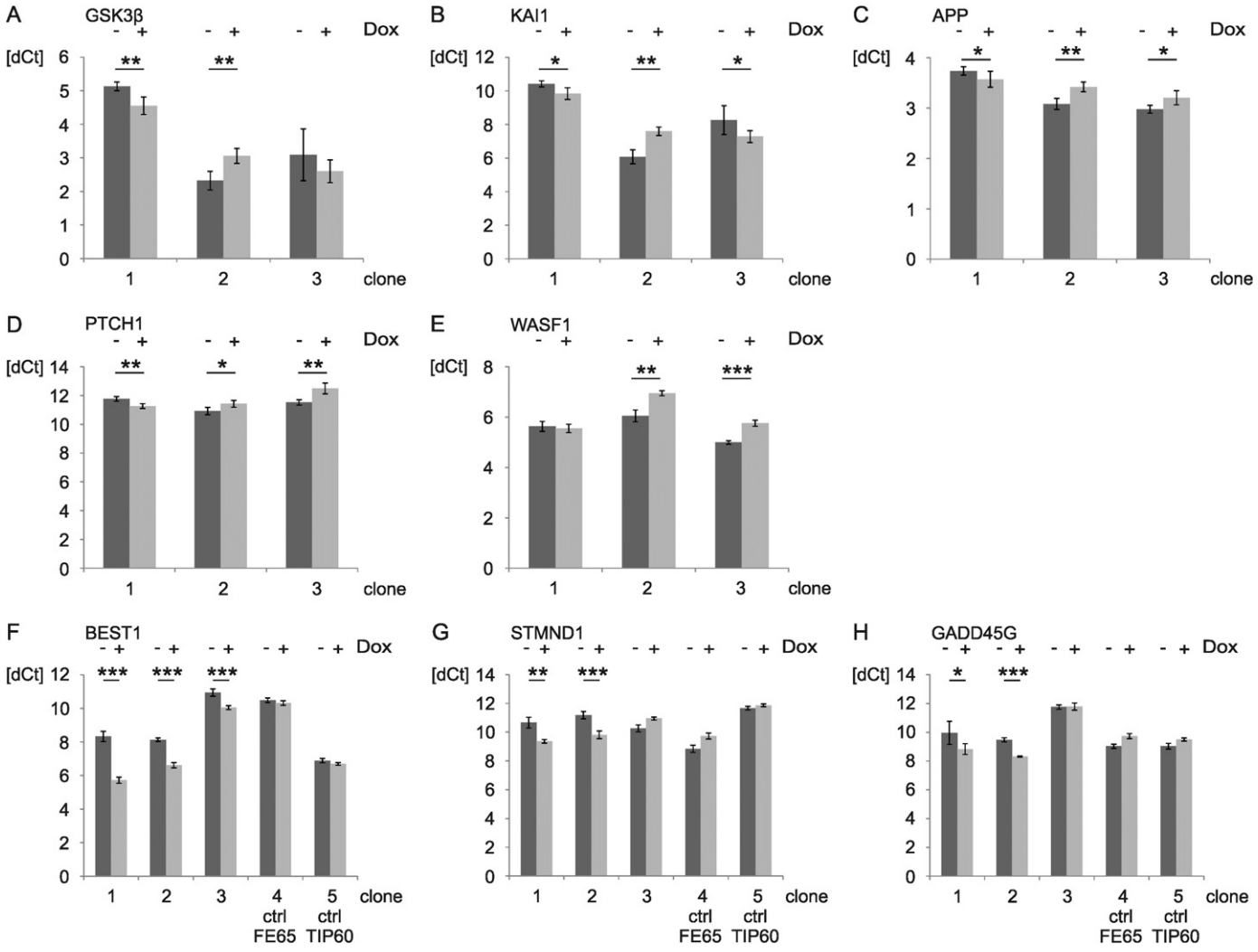

Fig. 3. Controversially discussed APP-dependent targets do not demonstrate convincing regulation in the nuclear sphere model but new FE65/TIP60-dependent target genes were identified. Potential APP (AICD)-dependently regulated genes were analyzed in cells with induced *FE65/TIP60* expression (+Dox) vs. controls (no induction, −Dox). Although in part significant regulations were found, none of the discussed targets revealed a stringent regulation in three different clones as the direction of regulation was opposed, e.g. *GSK3β* up-regulation in clone 1, but down-regulation in clone 2. In detail, *GSK3β* (A) revealed a regulation of 1.54 (±0.3, s.d.) in clone 1, 0.62 (±0.14, s.d.) in clone 2, and 1.61 (±0.82, s.d.) in clone 3. (B) *KAI1* (clone 1: 1.55 (±0.42, s.d.)/clone 2: 0.4 (±0.12, s.d.)/clone 3: 2.34 (±1.38, s.d.)). (C) *APP* (clone 1: 1.13 (±0.14, s.d.)/clone 2: 0.8 (±0.08, s.d.)/clone 3: 2.86 (±0.09, s.d.)). (D) *PTCH1* (clone 1: 1.43 (±0.22, s.d.)/clone 2: 0.72 (±0.16, s.d.)/clone 3: 0.53 (±0.15, s.d.)). (E) *WASF1* (clone 1: 1.07 (±0.18, s.d.)/clone 2: 0.54 (±0.09, s.d.)/clone 3: 0.59 (±0.05, s.d.)). After mRNA-array, potential candidate genes were validated with qPCR in cells with induced *FE65/TIP60* expression vs. controls. Furthermore, cells that only over-expressed FE65 (ctrl FE65) or TIP60 (ctrl TIP60) were used as controls to show the dependence of regulation upon *FE65/TIP60* co-expression. All of the shown candidates were significantly up-regulated in clones 1 and 2. Except of *BEST1* which was also significantly up-regulated in clone 3, the candidates were opposingly or not significantly regulated in clone 3 as well as in the FE65 and TIP60 controls. In detail, *BEST1* (F) revealed a regulation of 6.11 (±1.50, s.d.) in clone 1, 2.89 (±0.97, s.d.) in clone 2, 1.85 (±0.30, s.d.) in clone 3, 1.11 (±0.15, s.d.) in clone 4, and 1.15 (±0.12, s.d.) in clone 5. (G) *STMND1* (clone 1: 2.46 (±0.68, s.d.)/clone 2: 2.58 (±0.64, s.d.)/clone 3: 0.62 (±0.11, s.d.)/clone 4: 0.58 (±0.13, s.d.)/clone 5: 0.87 (±0.09, s.d.)). (H) *GADD45G* (clone 1: 2.60 (±1.62, s.d.)/clone 2: 2.23 (±0.22, s.d.)/clone 3: 0.97 (±0.20, s.d.)/clone 4: 0.61 (±0.10, s.d.)/clone 5: 0.73 (±0.11, s.d.)). *: $p < 0.05$, **: $p < 1 \times 10^{-4}$, ***: $p < 1 \times 10^{-8}$.

3.2. Nuclear spheres do not reveal consistent regulation of discussed target genes GSK3β, KAI1, APP, PTCH1 and WASF1

The APP intracellular domain has been linked to the regulation of the genes GSK3β [19], KAI1 [18], APP [16], and more recently to PTCH1 [31], and WASF1 [32]. As the central mechanism of AICD (APP) related signal transduction is the nuclear translocation of FE65 and subsequent generation of an FE65/TIP60 complex, we studied putative regulation of the described targets in the inducible nuclear sphere cell culture model. However, all potential targets failed in the qPCR analysis (Fig. 3A–E). Indeed, some targets revealed significant results in all studied clones (e.g. KAI1, Fig. 3B), but direction of regulation was opposed. Speculating that reverse regulation could be the consequence of varying FE65 to TIP60 (over-expression) ratios in the different clones (F > T or T > F), we re-addressed the obtained data as clone 3 behaves different to clones 1 and 2. Although all studied clones revealed significant induction of FE65 and TIP60, the amount of induction of a single gene was different. As a consequence, TIP60 was induced to a higher extent in clones 1 and 2 but to a lesser extent in clone 3, in that FE65 demonstrated higher induction (compare Fig. 2E).

However, for all targets in Fig. 3A–E regulation in clone 1 was opposed to that in clone 2 (but clones 1 and 2 behave equal in FE65/TIP60 ratio) pointing to the fact that more stringent parameters are needed to denote studied targets as a "real candidate". Derived from these results, we claimed for the planned transcriptomics study and subsequent qPCR based validation an regulation factor of more than 1.8 (or less than 0.55 respectively), an identical regulation course in clones 1 and 2, and statistical significance as combined criteria for potential new sphere-dependent regulated genes. Clone 3 was excluded from these criteria as a consequence of the different induction ratio (FE65 > TIP60).

3.3. Transcriptome analysis and subsequent qPCR validation revealed strong nuclear sphere-dependent induction of BEST1, STMND1, and GADD45G

The transcriptome of induced vs. non-induced cells was studied using Agilent whole genome expression microarrays. Following data analysis 27 transcripts revealed a significant regulation with a factor of more than 2.5 fold regulation (Table 1), which were subsequently all tested by qPCR. Overexpressed FE65 (APBB1) and TIP60 (KAT5) were found up-regulated and served as an internal control. Besides the nuclear sphere clone (clone 1), which was used for the microarray study, two additional (nuclear sphere positive) clones were included in the qPCR study: clone 2, which revealed less induction of FE65/TIP60 but with the same induction ratio (TIP60 was induced to a higher extent than FE65) and clone 3, which revealed opposed induction ratio (FE65 was induced to a higher extent than TIP60). Finally, a control clone inducible for FE65 alone and another one, inducible for TIP60, was included. All results from the qPCR analysis are given in Table 1. After application of the stringent qPCR selection criteria (as a consequence of the discussed target gene experiments (see above and Fig. 3A–E)), only 3 candidates sustained the predicate "real candidate": BEST1, STMND1, and GADD45G.

Bestrophin 1 (BEST1), a calcium-dependent chloride channel, demonstrated the highest regulation of all candidates in the studied clones (Fig. 3F). Consistently, no regulation of BEST1 was found in the control clones that are inducible for either FE65 or TIP60 alone pointing to the relevance of nuclear spheres for its regulation. The induction ratio of FE65 to TIP60 revealed no impact on BEST1 regulation as clone 3 (FE65 induction > TIP60 induction) demonstrated significant up-regulation of the candidate as well.

STMND1, the stathmin domain containing protein 1, revealed strong up-regulation in clones 1 and 2, but down-regulation in clone 3 putatively pointing to the relevance of the FE65/TIP60 ratio for the induction of this target transcript. Consistently, the control clones showed no effect on STMND1 regulation.

GADD45G, the growth arrest and DNA-damage-inducible protein gamma, highlighted significant induction in clones 1 and 2, but no regulation in clone 3 and in the controls. Thus, GADD45G might be nuclear sphere-dependent transcribed only if TIP60 induction exceeds that of FE65. Nevertheless, both proteins (FE65 and TIP60) are necessary for the induction of this target transcript. As for the other "real candidates", GADD45G revealed no expression changes in the control clones.

Considering all targets studied in this work indicates the potential importance of APP-dependently generated nuclear spheres in neurodegeneration. However, studying gene expression changes is challenging as many factors might be involved in its regulation. Studying nuclear sphere-dependent regulations might be even more defying — at least

Table 1
Candidate target genes of the FE65/TIP60 complex. Clone 1 was subjected to an mRNA array in order to identify potential target genes that are regulated by the FE65/TIP60 complex. Potential candidates were selected based on the fold change (FC) from the array data and targets with an array FC > 2.5 were considered for validation. Not annotated entries and entries with array signal raw-values < 100 were removed from the list. Furthermore, potential candidates were selected upon ingenuity pathway analysis (entries below the bold line, according to [33]). Over-expressed *FE65* (APBB1) and *TIP60* (KAT5) are shown in bold. All candidates were used for validation with qPCR in clone 1. Entries with empty cells were not analyzed in the respective samples as these candidates were not considered interesting after further data analysis. The line "(over-)expression" shows the qPCR regulation factors for *FE65* (F) and *TIP60* (T). In general FC qPCR-values > 1.8 were considered regulated.

(Over-)expression		Clone 1				Clone 2		Clone 3		Clone 4 (ctrl FE65)		Clone 5 (ctrl TIP60)	
				F: 4.59	T: 9.13	F: 2.01	T: 3.22	F: 5.03	T: 2.28	F: 1.93	T: 1.02	F: 1.23	T: 2.91
Gene symbol	Ref Seq Accession	FC array	p-Value	FC qPCR	p-Value	FC qPCR	p-Value	FC qPCR	p-Value	FC qPCR	p-Value	FC qPCR	p-Value
KAT5	**NM_006388**	**10.28**	**2.93E−06**	**9.13**	**2.53E−17**	**3.22**	**3.39E−06**	**2.28**	**4.64E−10**	**1.02**	**8.38E−01**	**2.91**	**5.11E−16**
RIMKLB	NM_020734	5.38	2.73E−06	2.35	8.89E−09	1.18	1.30E−06						
NEURL3	NM_001285486	4.24	1.65E−05	3.66	8.65E−05	1.60	1.21E−06	0.35	1.88E−07	1.25	3.74E−01		
KIAA0408	NM_014702	4.24	1.91E−05	5.50	1.23E−27	1.72	4.49E−09	0.99	8.49E−01	0.86	1.51E−01		
APBB1	**NM_001164**	**4.05**	**4.26E−06**	**4.59**	**1.69E−14**	**2.01**	**4.25E−11**	**5.03**	**6.80E−15**	**1.93**	**1.97E−07**	**1.23**	**2.02E−05**
BEST1	NM_004183	3.82	1.08E−05	6.11	1.92E−13	2.89	3.41E−14	1.85	9.66E−09	1.11	2.02E−03	1.15	1.34E−03
STMND1	NM_001190766	3.37	1.41E−05	2.46	2.87E−08	2.58	4.28E−09	0.62	8.64E−07	0.58	1.15E−06	0.87	2.35E−03
NPPB	NM_002521	3.21	1.23E−04	1.14	6.70E−01								
SNHG12	NR_024127	3.17	3.29E−06	3.68	6.94E−11	0.85	1.42E−04	1.01	1.00E + 00				
BEX1	NM_018476	3.09	4.49E−05	0.64	5.84E−04								
MATN1-AS1	NR_034182	3.03	3.84E−06	1.45	1.81E−04								
TMEM198	NM_001005209	3.03	4.01E−06	2.14	2.10E−08	1.61	4.23E−07	0.82	1.01E−04	0.65	4.34E−04	0.73	5.10E−07
PVT1	NR_003367	3.03	3.66E−06	2.22	8.85E−08	2.20	4.66E−14	1.24	4.49E−03	0.55	7.67E−09	0.97	5.77E−01
MMP24	NM_006690	3.00	1.21E−04	1.04	6.91E−01								
KRT80	NM_182507	2.85	1.51E−05	2.66	6.45E−09	0.91	1.73E−01						
STMN4	NM_030795	2.81	3.30E−05	4.89	1.49E−10	1.21	1.45E−02	1.28	2.11E−02	1.32	3.04E−05	0.94	4.61E−01
LOC643201	NR_036494	2.79	7.58E−06	2.77	4.17E−09	2.16	2.72E−10	0.95	6.78E−01	0.40	1.00E−03		
CYTIP	NM_004288	2.77	5.18E−05	3.27	2.32E−21	0.99	9.31E−01	0.48	6.46E−04				
XPA	NR_027302	2.76	3.69E−05	2.75	2.93E−09	1.19	6.92E−03						
EMC9	XR_245688	2.71	1.44E−05	4.82	6.05E−13	1.75	1.70E−09	0.88	6.48E−02	0.63	3.75E−05	0.81	1.56E−04
MIR7-3HG	NR_027148	2.70	1.49E−04	4.96	1.11E−12	1.17	1.44E−02	1.18	1.06E−01	0.72	2.90E−06	1.08	1.38E−01
LRP5L	NM_182492	2.69	6.17E−06	1.78	1.98E−04								
PHF21B	NM_138415	2.68	6.87E−06	4.50	7.10E−13	0.76	1.63E−07	0.78	2.70E−05				
WISP2	NM_003881	2.65	2.91E−05	1.24	2.09E−03								
KCNN4	NM_002250	2.64	2.61E−05	6.19	3.55E−14	1.10	2.35E−01	1.65	1.55E−03				
PTPRH	NM_002842	2.58	5.69E−05	3.86	3.18E−22	0.99	8.98E−01	0.97	6.99E−01				
SNAP25	NM_003081	2.51	6.37E−05	7.46	1.33E−08	0.88	4.43E−01	0.87	3.61E−01				
ETV5	NM_004454	2.64	6.11E−05	3.78	4.74E−25	0.69	4.68E−07	1.33	1.74E−05				
PER2	NM_022817	2.07	1.45E−05	3.94	1.16E−17	0.48	4.71E−07	0.88	3.62E−02				
CREB5	NM_182898	1.94	1.64E−05	1.92	1.34E−07								
NFKB2	NM_001288724	1.85	6.16E−05	2.97	1.56E−11	0.82	3.22E−03						
FOS	NM_005252	0.55	1.13E−04	1.23	8.41E−03								
SF1	ENST00000463343[a]	0.55	2.30E−05	0.61	1.79E−07								
GADD45G	NM_006705	1.79	1.36E−04	2.60	4.08E−09	2.23	6.61E−14	0.97	7.14E−01	0.61	3.70E−07	0.73	1.32E−05
ZMYND8	ENST00000468376[a]	0.57	1.39E−04	1.18	4.36E−02								

[a] No Ref Seq Accession was available, therefore the ensemble accession is provided.

the time-dependent structural alterations, the growth of small spheres and fusion to larger complexes, point to a great number of factors involved in the regulation of these nuclear components. Nevertheless, using the mentioned nuclear sphere induction model, we were able to identify new highly reliable target genes, which might contribute to Alzheimer's disease.

4. Discussion

Nuclear spheres, so far studied in cell culture models, were suggested to play a pivotal role in neurodegeneration [11]. The aggregates in the cellular nucleus are probably generated in dependence of the amyloid precursor protein cleavage or modification, but the precise mechanism remains unclear. In addition, there is no proof for their existence in the human brain until now, which might be the consequence of the nuclear sphere short lifespan (growth and fusion within short time) and challenging technical difficulties. For example, the detection of the APP intracellular domain (AICD) as a component of the spheres was reported to be not accessible to antibodies putatively as a consequence of the big macromolecular complex [12]. Nevertheless, the hypothesis of an APP-dependent nuclear signaling pathway, which could cause cell death in the human brain, corresponds to a highly interesting model as a cause for neurodegeneration.

Another consequence of the short nuclear sphere lifespan and its toxic character is the disability to develop reliable models. Over the last 3 years, we could not establish a stable over-expression model, also not with just moderate over-expression. Now, we were able to establish an FE65/TIP60 (Doxycycline) inducible cell culture model for the first time. As expected, at about 18 h after induction spheres could be monitored in the nucleus. Notably, spheres can also be observed by simple expression of FE65 but to a very low extent (<1%) potentially depending on endogenous TIP60 levels or additional yet unknown factors. In order to develop a suitable model, which can be studied by biochemical assays, co-induction of TIP60 is needed. Thus, the histone acetyltransferase takes over the role of a sphere enhancer in the described model and it becomes clear that the nuclear translocation of FE65 is the main switch in this story.

Anyhow, the interaction of FE65 and TIP60 in the nucleus, which has been described to depend on the PTB1 domain in FE65 and the NKSY motif in TIP60 [13], is an important prerequisite for the functional meaning of nuclear spheres. This fact can not only be concluded from the gene expression changes, which were assayed in this study, but already from the FE65 protein pattern in the different clones that were generated. Notably, only clones that reveal co-induction of both proteins demonstrated a significant cleavage of the full-length FE65 protein pointing to the relevance of functional active spheres (composed of FE65 AND TIP60) in protein degradation and potentially cell death. Putative FE65(−EGFP) cleavage products were detectable with a molecular weight of about 80 and 62 kDa in size, which might be a consequence of the described caspase-dependent [34] or endoproteolytic [35] FE65 cleavage or a combination of both. Mass spectrometry analysis of respective FE65 signals points to the fact that cleavage occurs from N- as well as from the C-terminus at specific sites of the protein FE65-EGFP taking the shift of 35 kDa, the first tryptic peptide at residue 134, and the last at residue 820 into consideration (compare Fig. 2C). The same is true for the small 62 kDa FE65 fragment.

The ongoing discussion of putative AICD-dependent target genes prompted us to study some candidates in the nuclear sphere model, again in the assumption that the nuclear aggregates correspond to the final step in APP signal transduction. We were pleasantly surprised when studying GSK3β, APP, KAI1, PTCH1 and WASF1 in clone 1, as all candidates revealed the reported up-regulation except for WASF1. Accordingly, we were highly disappointed after extending the study to clones 2 and 3 that revealed again mostly significant results but the opposite regulation direction. The easiest interpretation of the obtained results would be to designate these candidates as unspecific and to claim more stringent analysis parameter for qPCR related results in our cell model, which we also applied in the ongoing study. On the other hand, the story might be even more complicated and additional factors as yet unknown other nuclear sphere components might play a role for gene expression changes, which might be different from one stable clone to the other. It is not possible to solve this question at this time but at least, our results explain in part the highly controversial discussion of target genes and different findings in the field. In principle, it seems comprehensible that the nuclear complex can regulate gene expression in both directions, assuming that it acts as a transcriptional co-regulator. In addition, when screening the literature for proponents and repudiators of APP-dependent nuclear signal transduction it is striking that those, who describe gene expression effects, mostly work with models, in that nuclear aggregates (comparable to nuclear spheres) were proven or highly probable [19,36,16]. In contrast, in other work that do not show any impact on target genes discussed so far, just AICD levels or APP cleavage was modified [37,38,10]. This points to the hypothesis that the pure APP intracellular domain is not critical for nuclear signal transduction, although it might be transported into the nucleus in a piggyback-like (and thus probably unspecific) mechanism. However, other events at the C-terminal domain of APP might be responsible for signaling, especially phosphorylation. Notably, APP phosphorylations at T668 and Y682 (APP695 numbering) have been widely discussed to be responsible for FE65 interaction strength and by implication for FE65 translocation to the nucleus [4–6,39]. Interestingly, the T668 phosphorylation has also been reported to be significantly modified in Alzheimer's disease (AD) compared to controls [40,41].

The application of the addressed highly stringent qPCR analysis data to our subsequent screening experiment resulted in the consequence that only a very limited number of differentially regulated genes were selected for validation experiments. Amongst, bestrophin 1 (BEST1) was the most reliable putative new target gene with the highest up-regulation in all studied controls, but no effects in the single FE65 or single TIP60 inducible clones. As for the discussed FE65 cleavage pattern, also these results point to the relevance of nuclear sphere generation (TIP60 as sphere enhancer) for signaling function. The BEST1 ion channel was recently described to be involved in the abnormal release of GABA impairing memory in a mouse model of AD [42] fitting to other results showing that GABA is elevated in the cerebrospinal fluid of individuals with AD [43]. Thus, our study might reveal the missing link between AD associated neurotransmitter changes and the amyloid precursor protein.

Besides STMND1 — a protein, which has not been studied extensively so far, the growth arrest and DNA-damage-inducible protein gamma (GADD45G) was found upregulated in clones with FE65/TIP60 induction (TIP60 > FE65) but not in the control clones. GADD45G has been described to be involved in the cell cycle control by activating the S and G2/M checkpoints [44]. Thus, it fits to the discussed role of nuclear spheres in cell cycle re-entry [11]. As GADD45G is a nuclear protein, it might also be another component of nuclear spheres, which needs to be studied in near future.

5. Conclusions

Our work demonstrates that nuclear spheres have a remarkable impact on cellular gene expression changes and that it is worth to study the potential impact of these aggregates in neurodegeneration in detail. Of course, the proof of the existence of nuclear spheres in the human brain is pending. This might be solved by the identification of new proteins involved in the nuclear spheres like the potential candidate GADD45G from this study or the BLM from previous work [11]. Moreover, the APP-dependent generation of nuclear spheres and its suggested regulation by phosphorylation needs to be studied more precisely. Our work was able to identify new highly reliable nuclear sphere regulated genes, but –of course– also its validation is needed not only by other labs but also in additional models. Finally, further

validation of presented differentially regulated genes might also open the door for new therapeutic treatment strategies in the future.

Acknowledgment

This work was funded by FoRUM (Forschungsförderung Ruhr-Universität Bochum Medizinische Fakultät) F800-2014, MERCUR (Mercator Research Center Ruhr) AN-2013-0024, and DFG (Deutsche Forschungsgemeinschaft) MU3525/3.

Appendix A. Supplementary data

Supplementary data to this article can be found online at http://dx.doi.org/10.1016/j.cellsig.2015.10.019.

References

[1] R. Vassar, BACE1: the beta-secretase enzyme in Alzheimer's disease, Journal of molecular neuroscience: MN 23 (2004) 105–114.
[2] B. de. Strooper, Aph-1, Pen-2, and Nicastrin with Presenilin generate an active gamma-Secretase complex, Neuron 38 (2003) 9–12.
[3] G. Schettini, S. Govoni, M. Racchi, G. Rodriguez, Phosphorylation of APP–CTF–AICD domains and interaction with adaptor proteins: signal transduction and/or transcriptional role—relevance for Alzheimer pathology, J. Neurochem. 115 (2010) 1299–1308.
[4] K. Ando, K.I. Iijima, J.I. Elliott, Y. Kirino, T. Suzuki, Phosphorylation-dependent regulation of the interaction of amyloid precursor protein with Fe65 affects the production of beta-amyloid, J. Biol. Chem. 276 (2001) 40353–40361.
[5] K.-A. Chang, H.-S. Kim, T.-Y. Ha, J.-W. Ha, K.Y. Shin, Y.H. Jeong, J.-P. Lee, C.-H. Park, S. Kim, T.-K. Baik, et al., Phosphorylation of amyloid precursor protein (APP) at Thr668 regulates the nuclear translocation of the APP intracellular domain and induces neurodegeneration, Mol. Cell. Biol. 26 (2006) 4327–4338.
[6] T. Nakaya, T. Suzuki, Role of APP phosphorylation in FE65-dependent gene transactivation mediated by AICD, Genes to cells: devoted to molecular & cellular mechanisms 11 (2006) 633–645.
[7] W.T. Kimberly, J.B. Zheng, S.Y. Guénette, D.J. Selkoe, The intracellular domain of the beta-amyloid precursor protein is stabilized by Fe65 and translocates to the nucleus in a notch-like manner, J. Biol. Chem. 276 (2001) 40288–40292.
[8] G. Minopoli, P.d. Candia, A. Bonetti, R. Faraonio, N. Zambrano, T. Russo, The beta-amyloid precursor protein functions as a cytosolic anchoring site that prevents Fe65 nuclear translocation, J. Biol. Chem. 276 (2001) 6545–6550.
[9] X. Cao, T.C. Südhof, Dissection of amyloid-beta precursor protein-dependent transcriptional transactivation, J. Biol. Chem. 279 (2004) 24601–24611.
[10] E. Waldron, S. Isbert, A. Kern, S. Jaeger, A.M. Martin, S.S. Hébert, C. Behl, S. Weggen, B. de Strooper, C.U. Pietrzik, Increased AICD generation does not result in increased nuclear translocation or activation of target gene transcription, Exp. Cell Res. 314 (2008) 2419–2433.
[11] A. Schrötter, T. Mastalski, F.M. Nensa, M. Neumann, C. Loosse, K. Pfeiffer, F.E. Magraoui, H.W. Platta, R. Erdmann, C. Theiss, et al., FE65 regulates and interacts with the Bloom syndrome protein in dynamic nuclear spheres — potential relevance to Alzheimer's disease, J. Cell Sci. 126 (2013) 2480–2492.
[12] U. Konietzko, Z.V. Goodger, M. Meyer, B.M. Kohli, J. Bosset, D.K. Lahiri, R.M. Nitsch, Co-localization of the amyloid precursor protein and Notch intracellular domains in nuclear transcription factories, Neurobiol. Aging 31 (2010) 58–73.
[13] X. Cao, T.C. Südhof, A transcriptionally [correction of transcriptively] active complex of APP with Fe65 and histone acetyltransferase Tip60, Science 293 (2001) 115–120.
[14] T. Müller, A. Schrötter, C. Loosse, K. Pfeiffer, C. Theiss, M. Kauth, H.E. Meyer, K. Marcus, A ternary complex consisting of AICD, FE65, and TIP60 down-regulates Stathmin1, Biochim. Biophys. Acta 1834 (2013) 387–394.
[15] Z.V. Goodger, L. Rajendran, A. Trutzel, B.M. Kohli, R.M. Nitsch, U. Konietzko, Nuclear signaling by the APP intracellular domain occurs predominantly through the amyloidogenic processing pathway, J. Cell Sci. 122 (2009) 3703–3714.
[16] R.C. von Rotz, B.M. Kohli, J. Bosset, M. Meier, T. Suzuki, R.M. Nitsch, U. Konietzko, The APP intracellular domain forms nuclear multiprotein complexes and regulates the transcription of its own precursor, J. Cell Sci. 117 (2004) 4435–4448.
[17] T. Müller, C.G. Concannon, M.W. Ward, C.M. Walsh, A.L. Tirniceriu, F. Tribl, D. Kögel, J.H.M. Prehn, R. Egensperger, Modulation of gene expression and cytoskeletal dynamics by the amyloid precursor protein intracellular domain (AICD), Mol. Biol. Cell 18 (2007) 201–210.
[18] S.H. Baek, K.A. Ohgi, D.W. Rose, E.H. Koo, C.K. Glass, M.G. Rosenfeld, Exchange of N-CoR corepressor and Tip60 coactivator complexes links gene expression by NF-kappaB and beta-amyloid precursor protein, Cell 110 (2002) 55–67.
[19] H.-S. Kim, E.-M. Kim, J.-P. Lee, C.H. Park, S. Kim, J.-H. Seo, K.-A. Chang, E. Yu, S.-J. Jeong, Y.H. Chong, et al., C-terminal fragments of amyloid precursor protein exert neurotoxicity by inducing glycogen synthase kinase-3beta expression, FASEB J. 17 (2003) 1951–1953.
[20] D.P. Hanger, K. Hughes, J.R. Woodgett, J.P. Brion, B.H. Anderton, Glycogen synthase kinase-3 induces Alzheimer's disease-like phosphorylation of tau: generation of paired helical filament epitopes and neuronal localisation of the kinase, Neurosci. Lett. 147 (1992) 58–62.
[21] S. Huysseune, P. Kienlen-Campard, J.-N. Octave, Fe65 does not stabilize AICD during activation of transcription in a luciferase assay, Biochem. Biophys. Res. Commun. 361 (2007) 317–322.
[22] M. Stante, G. Minopoli, F. Passaro, M. Raia, L.D. Vecchio, T. Russo, Fe65 is required for Tip60-directed histone H4 acetylation at DNA strand breaks, Proc. Natl. Acad. Sci. U. S. A. 106 (2009) 5093–5098.
[23] I. Szumiel, N. Foray, Chromatin acetylation, β-amyloid precursor protein and its binding partner FE65 in DNA double strand break repair, Acta Biochim. Pol. 58 (2011) 11–18.
[24] A. Kinoshita, C.M. Whelan, O. Berezovska, B.T. Hyman, The gamma secretase-generated carboxyl-terminal domain of the amyloid precursor protein induces apoptosis via Tip60 in H4 cells, J. Biol. Chem. 277 (2002) 28530–28536.
[25] S. Ryu, F. Teles, G. Minopoli, T. Russo, M.G. Rosenfeld, Y. Suh, An epigenomic role of Fe65 in the cellular response to DNA damage, Mutat. Res. 776 (2015) 40–47.
[26] P. Bruni, G. Minopoli, T. Brancaccio, M. Napolitano, R. Faraonio, N. Zambrano, U. Hansen, T. Russo, Fe65, a ligand of the Alzheimer's beta-amyloid precursor protein, blocks cell cycle progression by down-regulating thymidylate synthase expression, J. Biol. Chem. 277 (2002) 35481–35488.
[27] K.A. Reidegeld, M. Eisenacher, M. Kohl, D. Chamrad, G. Körting, M. Blüggel, H.E. Meyer, C. Stephan, An easy-to-use Decoy Database Builder software tool, implementing different decoy strategies for false discovery rate calculation in automated MS/MS protein identifications, Proteomics 8 (2008) 1129–1137.
[28] J. Uszkoreit, A. Maerkens, Y. Perez-Riverol, H.E. Meyer, K. Marcus, C. Stephan, O. Kohlbacher, M. Eisenacher, PIA: An Intuitive Protein Inference Engine with a Web-Based User Interface, J. Proteome Res. 14 (2015) 2988–2997.
[29] R.A. Kley, A. Maerkens, Y. Leber, V. Theis, A. Schreiner, P.F.M. van der Ven, J. Uszkoreit, C. Stephan, S. Eulitz, N. Euler, et al., A combined laser microdissection and mass spectrometry approach reveals new disease relevant proteins accumulating in aggregates of filaminopathy patients. Mol. Cell. Proteomics 12 (2013) 215–227.
[30] K.J. Livak, T.D. Schmittgen, Analysis of relative gene expression data using real-time quantitative PCR and the 2(−Delta Delta C(T)) method, Methods (San Diego, Calif.) 25 (2001) 402–408.
[31] M. Raychaudhuri, D. Mukhopadhyay, AICD Overexpression in Neuro 2A Cells Regulates Expression of PTCH1 and TRPC5, Int. J. Alzheimers Dis. 2011 (2011).
[32] I. Ceglia, C. Reitz, J. Gresack, J.-H. Ahn, V. Bustos, M. Bleck, X. Zhang, G. Martin, S.M. Simon, A.C. Nairn, et al., APP intracellular domain-WAVE1 pathway reduces amyloid-β production, Nat. Med. 21 (2015) 1054–1059.
[33] T. Müller, A. Schrötter, C. Loosse, S. Helling, C. Stephan, M. Ahrens, J. Uszkoreit, M. Eisenacher, H.E. Meyer, K. Marcus, Sense and nonsense of pathway analysis software in proteomics, J. Proteome Res. 10 (2011) 5398–5408.
[34] K. Saeki, Y. Nose, N. Hirao, R. Takasawa, S.-I. Tanuma, Amyloid precursor protein binding protein Fe65 is cleaved by caspases during DNA damage-induced apoptosis, Biol. Pharm. Bull. 34 (2011) 290–294.
[35] Q. Hu, L. Wang, Z. Yang, B.H. Cool, G. Zitnik, G.M. Martin, Endoproteolytic cleavage of FE65 converts the adaptor protein to a potent suppressor of the sAPPalpha pathway in primates, J. Biol. Chem. 280 (2005) 12548–12558.
[36] F. Telese, P. Bruni, A. Donizetti, D. Gianni, C. D'Ambrosio, A. Scaloni, N. Zambrano, M.G. Rosenfeld, T. Russo, Transcription regulation by the adaptor protein Fe65 and the nucleosome assembly factor SET, EMBO Rep. 6 (2005) 77–82.
[37] D. Aydin, M.A. Filippov, J.-A. Tschäpe, N. Gretz, M. Prinz, R. Eils, B. Brors, U.C. Müller, Comparative transcriptome profiling of amyloid precursor protein family members in the adult cortex, BMC Genomics 12 (2011) 160.
[38] S.S. Hébert, L. Serneels, A. Tolia, K. Craessaerts, C. Derks, M.A. Filippov, U. Müller, B. de Strooper, Regulated intramembrane proteolysis of amyloid precursor protein and regulation of expression of putative target genes, EMBO Rep. 7 (2006) 739–745.
[39] D. Zhou, N. Zambrano, T. Russo, L. D'Adamio, Phosphorylation of a tyrosine in the amyloid-beta protein precursor intracellular domain inhibits Fe65 binding and signaling, J. Alzheimers Dis. 16 (2009) 301–307.
[40] M.-S. Lee, S.-C. Kao, C.A. Lemere, W. Xia, H.-C. Tseng, Y. Zhou, R. Neve, M.K. Ahlijanian, L.-H. Tsai, APP processing is regulated by cytoplasmic phosphorylation, J. Cell Biol. 163 (2003) 83–95.
[41] R.-W. Shin, K. Ogino, A. Shimabuku, T. Taki, H. Nakashima, T. Ishihara, T. Kitamoto, Amyloid precursor protein cytoplasmic domain with phospho-Thr668 accumulates in Alzheimer's disease and its transgenic models: a role to mediate interaction of Abeta and tau, Acta Neuropathol. 113 (2007) 627–636.
[42] S. Jo, O. Yarishkin, Y.J. Hwang, Y.E. Chun, M. Park, D.H. Woo, J.Y. Bae, T. Kim, J. Lee, H. Chun, et al., GABA from reactive astrocytes impairs memory in mouse models of Alzheimer's disease, Nat. Med. 20 (2014) 886–896.
[43] S. Samakashvili, C. Ibáñez, C. Simó, F.J. Gil-Bea, B. Winblad, A. Cedazo-Mínguez, A. Cifuentes, Analysis of chiral amino acids in cerebrospinal fluid samples linked to different stages of Alzheimer disease, Electrophoresis 32 (2011) 2757–2764.
[44] M. Vairapandi, A.G. Balliet, B. Hoffman, D.A. Liebermann, GADD45b and GADD45g are cdc2/cyclinB1 kinase inhibitors with a role in S and G2/M cell cycle checkpoints induced by genotoxic stress, J. Cell. Physiol. 192 (2002) 327–338.